Author Manuscript

Author Manuscript

Author Manuscript

Author Manuscript

HHS Public Access

Author manuscript

Mol Cell. Author manuscript; available in PMC 2016 October 15.

Published in final edited form as:

Mol Cell. 2015 October 15; 60(2): 280–293. doi:10.1016/j.molcel.2015.09.011.

RFWD3-Dependent Ubiquitination of RPA Regulates Repair at Stalled Replication Forks

Andrew E.H. Elia[1,2], **David C. Wang**[1,2], **Nicholas A. Willis**[3], **Alexander P. Boardman**[1,2], **Ildiko Hajdu**[1], **Richard O. Adeyemi**[1], **Elizabeth Lowry**[1,2], **Steven P. Gygi**[4], **Ralph Scully**[3], and **Stephen J. Elledge**[1,*]

[1]Department of Genetics, Harvard Medical School, Division of Genetics, Brigham and Women's Hospital, Howard Hughes Medical Institute, Boston, MA 02115

[2]Department of Radiation Oncology, Massachusetts General Hospital, Boston, MA 02114

[3]Beth Israel Deaconess Medical Center, Harvard Medical School, Boston, MA 02215

[4]Department of Cell Biology, Harvard Medical School, Boston, MA 02115

Summary

We have used quantitative proteomics to profile ubiquitination in the DNA damage response (DDR). We demonstrate that RPA, which functions as a protein scaffold in the replication stress response, is multiply ubiquitinated upon replication fork stalling. Ubiquitination of RPA occurs on chromatin, involves sites outside its DNA binding channel, does not cause proteasomal degradation, and increases under conditions of fork collapse, suggesting a role in repair at stalled forks. We demonstrate that the E3 ligase RFWD3 mediates RPA ubiquitination. RFWD3 is necessary for replication fork restart, normal repair kinetics during replication stress, and homologous recombination (HR) at stalled replication forks. Mutational analysis suggests that multisite ubiquitination of the entire RPA complex is responsible for repair at stalled forks. Multisite protein group sumoylation is known to promote HR in yeast. Our findings now reveal a similar requirement for multisite protein group ubiquitination during HR at stalled forks in mammalian cells.

Graphical Abstract

*To whom correspondence should be addressed: Stephen J. Elledge: selledge@genetics.med.harvard.edu.

Publisher's Disclaimer: This is a PDF file of an unedited manuscript that has been accepted for publication. As a service to our customers we are providing this early version of the manuscript. The manuscript will undergo copyediting, typesetting, and review of the resulting proof before it is published in its final citable form. Please note that during the production process errors may be discovered which could affect the content, and all legal disclaimers that apply to the journal pertain.

Author Manuscript Author Manuscript Author Manuscript Author Manuscript

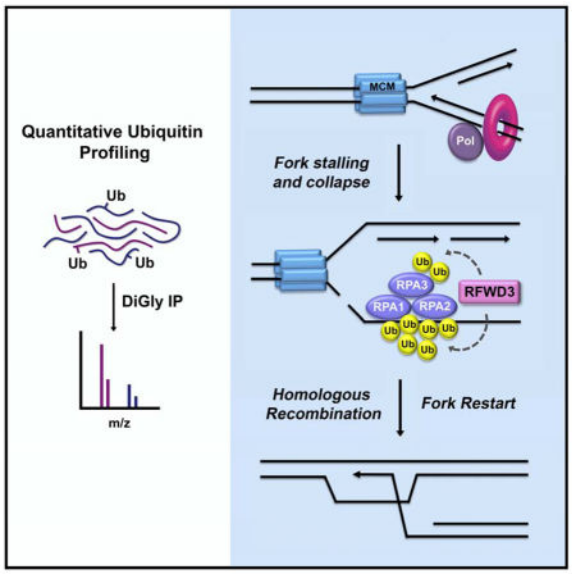

Introduction

The human genome is continuously exposed to toxic insults from environmental and endogenous sources. DNA lesions resulting from these insults must be repaired in order to maintain genomic stability. To coordinate repair with other cellular processes, such as cell cycle progression, replication, and transcription, cells have evolved an elaborate signaling network known as the DNA damage response (DDR) (Ciccia and Elledge, 2010; Sirbu and Cortez, 2013). Exquisite regulation of the DDR is mediated by numerous protein modifications, among which ubiquitination plays a crucial role (Bekker-Jensen and Mailand, 2011; Jackson and Durocher, 2013; Messick and Greenberg, 2009). Ubiquitin-dependent signaling regulates the double strand break (DSB) response, the Fanconi anemia (FA) pathway, nucleotide excision repair (NER), and post-replication repair. We have used quantitative proteomics to globally profile ubiquitination in the cellular responses to both replication stress and DSBs (Elia et al., 2015).

Cellular responses to replication stress and to DSBs are orchestrated by the two kinases ATR and ATM. Signaling by both kinases relies on central scaffold proteins that coordinate the assembly of multiprotein complexes at DNA damage sites. In the ATR pathway, the scaffold RPA binds single-stranded DNA (ssDNA) generated during replication fork stalling and recruits the factors ATRIP, RAD17, and RAD9 to promote ATR activation (Xu et al., 2008; Zou and Elledge, 2003; Zou et al., 2003). RPA also recruits factors necessary for the stabilization of stalled replication forks such as SMARCAL1 (Bansbach et al., 2009; Ciccia et al., 2009; Yuan et al., 2009; Yusufzai et al., 2009). In the ATM pathway, the histones H2AX and H2A serve as loading platforms at DSB sites in order to propagate signals generated by ATM. ATM-mediated phosphorylation of H2AX directly recruits MDC1 and its associated ubiquitin ligase RNF8, which drives accumulation of a second ubiquitin ligase RNF168 at DSB sites. Both RPA and H2AX thus serve as central hubs for kinase signaling, and both are DDR phosphorylation substrates themselves.

Author Manuscript Author Manuscript Author Manuscript Author Manuscript

Ubiquitination of H2A/H2AX has emerged as an important regulatory mechanism for ATM signal propagation and localization of repair factors to DSB sites (Doil et al., 2009; Huen et al., 2007; Mailand et al., 2007; Mattiroli et al., 2012; Stewart et al., 2009). RNF168-mediated ubiquitination of H2A/H2AX recruits 53BP1 and BRCA1, which promote non-homologous end joining (NHEJ) and homologous recombination (HR) repair at DSBs, respectively. Here, we show that multiple sites on all three subunits of the scaffold RPA are ubiquitinated in response to replication stress. RPA ubiquitination occurs on chromatin, does not cause proteasomal degradation, and increases under conditions of fork collapse, suggestive of a role in repair at stalled replication forks. We demonstrate that the E3 ligase RFWD3 is responsible for RPA ubiquitination and that RFWD3 is necessary for both the recovery of stalled replication forks and for HR at stalled forks. Notably, HR factors have increasingly been implicated in the stabilization and restart of stalled forks (Hashimoto et al., 2010; Petermann et al., 2010; Schlacher et al., 2011; Schlacher et al., 2012).

Regulatory ubiquitination of scaffold proteins in multiple repair pathways occurs on specific lysine residues. In the DSB response, for example, site-specific ubiquitination of H2A on K15 recruits 53BP1 through direct interaction with its UDR motif (Fradet-Turcotte et al., 2013). Similarly, PCNA ubiquitination on K164 functions during post-replication repair to promote translesion synthesis and template switching, while ubiquitination of FANCI/D2 on K523/K561 promotes interstrand crosslink repair in the FA pathway. Here, we demonstrate through mutational analysis that ubiquitination of numerous sites within multiple subunits of the RPA complex contribute to HR at stalled forks, similar to the requirement for multisite protein group sumoylation observed in yeast HR (Psakhye and Jentsch, 2012). Overall, these findings establish the requirement for multisite RPA ubiquitination in HR at stalled forks and demonstrate the utility of our proteomic datasets in elucidating additional pathways of ubiquitin-dependent signaling in the DDR.

Results

RPA is ubiquitinated on chromatin in response to ultraviolet radiation

To systematically investigate ubiquitination in the cellular responses to replication stress and DSBs, we performed ubiquitin remnant profiling and stable isotope labeling in cell culture (Figures 1A, S1A) as described in our companion manuscript (Elia et al., 2015). Heavy isotope labeled cells were left untreated while unlabeled light cells were treated with either UV or ionizing radiation. The ssDNA binding protein RPA1 was among proteins whose ubiquitination was most highly regulated in response to UV. We found 14 ubiquitination sites on RPA1 that increased at least two-fold following UV treatment (Figure 1B, Table S1). We validated RPA1 ubiquitination in response to the UV mimetic 4NQO by expressing His-tagged ubiquitin in cells, purifying ubiquitinated proteins under denaturing conditions, and immunoblotting for endogenous RPA1 (Figure 1C). RPA is a complex of three proteins (RPA1, RPA2, and RPA3), and our proteomic analyses also detected increased ubiquitination of RPA3 on three sites (Figure S1B). While we did not observe inducible RPA2 ubiquitination in these screens, possibly for technical reasons, purification of His-tagged ubiquitinated proteins demonstrated that RPA2 was also robustly ubiquitinated in response to 4NQO (Figure 1D). Thus, UV-induced ubiquitination occurs on a minimum of

Author Manuscript Author Manuscript Author Manuscript Author Manuscript

18 sites in the RPA complex. Notably, we were unable to detect inducible RPA1 or RPA2 ubiquitination upon overexposure of lysate immunoblots (data not shown), indicating that the fraction of RPA modified by ubiquitination is small. Low occupancy suggests RPA ubiquitination occurs locally in the vicinity of DNA damage.

RPA1 contains four OB-folds (oligonucleotide/oligosaccharide-binding folds) that constitute the majority of the protein (Figure 1F). The three C-terminal OB-folds bind DNA and are termed DBD-A, DBD-B, and DBD-C, while the first N-terminal OB-fold mediates interactions with proteins. We found that UV-induced sites of RPA1 ubiquitination were present in all four OB-folds. In principle, OB fold ubiquitination could serve to prevent RPA1 binding to DNA. To predict whether RPA1 ubiqutination within these folds disrupts interaction with DNA, we mapped ubiquitinated lysines onto a co-crystal structure of ssDNA bound to the DBD-A and DBD-B domains of RPA1 (Bochkarev et al., 1997). This structure shows that DNA lies in a channel formed by the two domains arrayed in tandem (Figure S2A). Two lysines line this channel (K263 and K343, Figure S2B), and neither is ubiquitinated in response to UV radiation (Figure 1B). Importantly, among the seven ubiquitinated lysines in DBD-A and DBD-B (Figure 1F), all are located outside the DNA-binding cleft (Figures 1G, S2C). This finding suggests that RPA ubiquitination does not directly disrupt DNA binding. Consistent with this idea, we found that association with chromatin was necessary for ubiquitination of RPA1 and RPA2 (Figure 1E). This result, along with our finding that RPA ubiquitination occupancy is low, supports the model that RPA is bound to DNA at sites of damage when ubiquitinated.

RPA ubiquitination occurs in response to replication fork stalling

UV and 4NQO can cause replication fork stalling but can also introduce S-phase independent lesions that activate NER pathways. To better understand what lesions stimulate RPA ubiquitination, we evaluated additional DNA damage agents. We found that 10 Gy IR did not induce RPA ubiquitination at 1 hour (Figure 2A), and this finding was confirmed by our proteomic data (Figure 2B, Table S1). The topoisomerase inhibitor camptothecin stimulated both RPA1 and RPA2 ubiquitination, suggesting the ubiquitination may be replication-dependent (Figure 2A). Hydroxyurea (HU) arrests replication forks through nucleotide pool depletion, and it elicited robust ubiquitination of both RPA1 and RPA2 (Figure 2C). We also found that polymerase inhibition with aphidicolin stimulated RPA1 and RPA2 ubiquitination (Figure 4C). These results suggest that fork stalling is sufficient for causing RPA ubiquitination.

Kinetic evaluation demonstrated that RPA1 and RPA2 ubiquitination occurred within 30 minutes of HU or 4NQO and continued to increase 2 hours after treatment (Figures 2C, 2D). Because these experiments involved continuous drug incubation and thus successively longer exposures to the insult, we also evaluated kinetics after a fixed dose of UV radiation. Again, we observed a steady increase in ubiquitination from 30 minutes to 2 hours (Figure 2E). Beyond 2 hours, HU-induced ubiquitination continued to increase further (Figure S1C). This increase may arise from the firing of additional replication origins as more cells enter S-phase, which may lead to more ssDNA generation as additional helicases uncouple from stalled polymerases. However, we also considered the possibility that RPA ubiquitination

Author Manuscript Author Manuscript Author Manuscript Author Manuscript

may be stimulated by the collapse of stalled replication forks. Combined ATR inhibition and HU treatment has been shown to induce DSB formation at stalled forks resulting in replication catastrophe (Toledo et al., 2013). As described in this report, we found that simultaneous ATR inhibition and HU treatment increased RPA2 S4/8 and T21 phosphorylation (Figure S1D) likely by activating ATM. Importantly, RPA ubiquitination was also increased under these conditions (Figure 2F), suggesting that fork collapse may contribute to RPA ubiquitination. Notably, these findings also suggest that ATR is not upstream of HU-induced RPA ubiquitination.

RPA ubiquitination does not lead to its degradation by the proteasome

To gain insight into the biological function of RPA ubiquitination, we evaluated whether RPA ubiquitination leads to its degradation by the proteasome. Given the small fraction of RPA that is modified by ubiquitination, it is not meaningful to examine changes in bulk RPA levels upon proteasome inhibition. Instead, one must interrogate the effects of proteasome inhibition specifically on the ubiquitinated RPA species. We therefore examined RPA ubiquitination using diGly proteomics in the presence of the proteasome inhibitor MG132. Heavy isotope labeled cells were treated with MG132 while light cells were treated with both MG132 and UV radiation (Figure 3A). For proteins whose UV-induced ubiquitination leads to degradation, such as CDC25A and SETD8, proteasomal inhibition will increase the detection of ubiquitinated peptides as measured by spectral counting (Figure S3A). We found that pre-treatment of cells with MG132 did not significantly increase the spectral counts for RPA ubiquitination (Figure S3B).

Furthermore, we found that MG132 strongly reduced the induction of both RPA1 and RPA3 ubiquitination upon UV radiation as determined by SILAC quantitation (Figures 3B and S3C, Table S1). It is known that, through ubiquitin pool depletion, proteasome inhibition can reduce the levels of non-degradative ubiquitination events in the nucleus that do not lead to proteasomal targeting (Dantuma et al., 2006; Mailand et al., 2007). Consistent with our proteomic results, we found that MG132 inhibited RPA2 and RPA1 ubiquitination as detected by pulldown of histidine-tagged ubiquitinated proteins (Figures 3C, S3D). This finding stands in significant contrast to the dramatic induction of ubiquitination observed for the known proteasomal substrate CDC25A upon MG132 treatment (Figure 3C). Together, these findings suggest that RPA ubiquitination does not lead to its degradation.

Linkage specificity for RPA polyubiquitination

Failure to induce proteasomal degradation suggested a role for RPA ubiquitination in cellular signaling. To examine ubiquitin linkage specificity, we expressed His-tagged wild type, K63R, K48R, and K6R ubiquitin in cells. We verified that these ubiquitin constructs were expressed at equivalent levels (Figure S3E) and purified ubiquitinated RPA by denaturing nickel pulldown. Notably, we did not observe a significant reduction in 4NQO- or HU-induced RPA1 or RPA2 ubiquitination with any of these mutants (Figures 3D, S3F). Interestingly, however, K63R mutation did cause the loss of a single ubiquitinated band (arrowhead in Figures 3F, 3D, S3F) representing likely di- or tri-ubiquitinated RPA1. This single band also disappeared upon depletion of the E2 conjugating enzyme UBC13 (Figures 3F, 3E, S3G), which is responsible for K63-linked polyubiquitination. Yet again, we

Author Manuscript Author Manuscript Author Manuscript Author Manuscript

detected no significant reduction in bulk RPA ubiquitination upon UBC13 depletion (Figures 3E, S3G). Nickel-purified polyubiquitin chains from cells expressing K63R His-ubiquitin may contain endogenous ubiquitin and consequently may not be homogeneous for the K63R mutant ubiquitin. However, loss of the exact same RPA1 band in both the K63R mutant ubiquitin and UBC13 depletion experiments (Figure 3F) argues that K63-linked polyubiquitination was functionally inhibited in both of these experiments. These results thus suggest that ubiquitination of RPA1 involves mixed linkage specificity and that neither RPA1 nor RPA2 ubiquitination involves predominantly K63 linkages.

The ubiquitin ligase RFWD3 mediates RPA ubiquitination

To determine the E3 ligase responsible for RPA ubiquitination, we immunoprecipitated HA-tagged RPA1 from cells and identified interacting proteins by mass spectrometry. In addition to binding RPA2 and RPA3, we found that RPA1 associated with four ubiquitin ligases: HERC2, HLTF, PRP19, and RFWD3 (Figure S4A). In depleting these candidate ligases, we discovered a surprising and pervasive artifact of siRNA transfection on exogenous transgene expression. Remarkably, certain siRNAs inhibited the expression of CMV-driven tagged ubiquitin. For example, we found that four siRNAs depleted PRP19 to the same extent yet differentially inhibited RPA ubiquitination. This inhibition of RPA ubiquitination correlated precisely with decreases in His-ubiquitin levels rather than PRP19 depletion (Figures S4B, S4C). We suspect that this artifact is mediated by the interferon response, which normally detects long double-stranded RNAs but is also known to occur with siRNAs (Nejepinska et al., 2012). Interferon can inhibit expression from exogenous CMV promoters (Harms and Splitter, 1995). Notably, this artifact was exceedingly common, occurring with 48% of all siRNAs that we examined for effects on RPA ubiquitination.

Among the other RPA-associated ligases, we found that depletion of only RFWD3 blocked RPA1 ubiquitination without affecting the expression of histidine tagged ubiquitin (Figure 4A and data not shown). Inhibition of HU, APH, or 4NQO-induced RPA1 ubiquitination occurred when transfecting three separate siRNAs (Figures 4A–D) and when transducing two unrelated shRNAs (Figures 4E, S4E), none of which affected exogenous ubiquitin expression. To find these five reagents, we screened a total of 12 siRNAs or shRNAs. Importantly, depletion of RFWD3 with these five reagents also abrogated ubiquitination of RPA2 (Figures 4B–E, S4E). Furthermore, the level of RFWD3 depletion correlated with inhibition of RPA ubiquitination (Figures 4D, S4E).

While the use of multiple RNAi reagents minimizes the likelihood of off-target RNAi effects (Adamson et al., 2012), we definitively ruled out this possibility by performing a rescue experiment with shRNA-resistant RFWD3. Complementation of RFWD3-depleted cells with shRNA-resistant RFWD3, unlike with an empty vector negative control, rescued HU-induced ubiquitination of both RPA1 and RPA2 (Figure 4E). Importantly, HU-induced levels of RPA1 and RPA2 ubiquitination increased with overexpression of RFWD3 (lane 7 in Figure 4E). Together, these results indicate that RFWD3 mediates the ubiquitination of both RPA1 and RPA2 in response to DNA damage.

Author Manuscript Author Manuscript Author Manuscript Author Manuscript

RFWD3 promotes the restart of stalled replication forks

Upon the restart of stalled replication forks after release from a HU-induced arrest, we observed complete loss of RPA ubiquitination two hours after release (Figure 5A), with RPA deubiquitination initiating as early as 30 minutes after release (Figure S5A). Correlation of RPA ubiquitination with actively stalled forks suggested that ubiquitination may function in the stabilization of stalled forks. Thus, we performed single DNA fiber analysis on cells depleted of RFWD3 (Figure 5B). Cells were pulse-labeled with the thymidine analog IdU for 20 minutes and then incubated with HU for 2 hours to arrest replication forks. Following HU washout, cells were labeled with another thymidine analog CldU for 25 minutes. Forks that restarted after HU removal are visualized as a stretch of IdU incorporation (red in Figure 5B) followed by a stretch of CldU incorporation (green in Figure 5B). Tracts of only IdU incorporation indicate stalled or collapsed forks, whereas tracts of only CldU incorporation represent new origins that fired after HU removal. We found that depletion of RFWD3 decreased fork restart, as indicated by a greater than two-fold reduction in fibers containing both IdU and CldU incorporation (Figure 5C), and this decrease was reversed by expression of siRNA-resistant RFWD3 (Figure 5D). These results suggest that RFWD3 promotes fork stability or restart upon replication stress.

RFWD3 stimulates homologous recombination at stalled replication forks

Factors involved in homologous recombination (HR) are known to stabilize and promote the restart of stalled replication forks in both yeast and human cells (Petermann and Helleday, 2010; Petermann et al., 2010; Schlacher et al., 2012). RPA functions in HR, and we wondered whether RFWD3's role in fork restart could be related to a potential function in HR repair at stalled forks. Supporting this possibility, HU-induced RPA ubiquitination was enhanced by ATR inhibition, suggesting that collapse of stalled forks may contribute to RPA ubiquitination (Figure 2F). To evaluate kinetics of repair at stalled forks, we examined γH2AX foci resolution after release from prolonged 24 hour HU treatment, which has been shown to induce DSBs at stalled forks (Petermann et al., 2010; Toledo et al., 2013). We found that RFWD3 depletion decreased the rate of γ-H2AX resolution, and importantly, expression of siRNA-resistant RFWD3 restored normal repair kinetics (Figure 5E). These results suggest that RFWD3 promotes DSB repair at collapsed forks.

We next sought to determine whether RFWD3 regulates homologous recombination. Given that RPA ubiquitination is stimulated by replication stress, we sought to examine HR specifically at stalled replication forks. To accomplish this, we used a recently described reporter in which six bacterial *Ter* sites interrupt an enhanced *GFP* gene inserted in the *ROSA26* locus of a mouse embryonic stem cell line (Figure 6A) (Willis et al., 2014). Expression of the bacterial Tus protein, which binds to the 6x*Ter* array, causes site-specific bidirectional replication fork arrest in these cells. Recombination of the stalled fork with a 5′ adjacent truncated GFP copy (Tr-GFP) generates wild type GFP that can be detected by flow cytometry. Abutting the *6xTer* array is an I-SceI endonuclease site, which allows for additional quantitation of HR induced by a chromosomal double strand break. We found that depletion of mouse RFWD3 using an siRNA pool reduced HR after both Tus-induced fork stalling and I-SceI double strand breaks (Figures 6B, 6C). These findings were validated using four individual siRNAs comprising the pool (Figures 6D, S5B). RFWD3 depletion

Author Manuscript Author Manuscript Author Manuscript Author Manuscript

was verified by RT-qPCR, and inhibition of HR correlated with the level of RFWD3 depletion (Figures 6D, S5C). Notably, RFWD3 depletion did not affect cell cycle progression (Figure S5D). These results demonstrate that RFWD3 promotes HR at stalled replication forks and provide a potential mechanism through which RFWD3 stimulates fork restart.

Evaluation of the role for RFWD3 in ATR pathway activation

ATR is known to promote both replication fork restart (Zeman and Cimprich, 2014) and homologous recombination (Adamson et al., 2012; Sorensen et al., 2005; Wang et al., 2004). We thus evaluated whether RFWD3 regulates the ATR signaling pathway. We initially examined phosphorylation of the ATR substrate RPA2, as we observed that the kinetics of RFWD3-induced RPA ubiquitination matched that for RPA2 phosphorylation, as determined by shifts in RPA2 mobility after treatment with HU, UV, or 4NQO (Figures 2C–E). This correlation suggested a causal relationship between RFWD3 function and RPA2 phosphorylation. Indeed, we found that RFWD3 depletion caused a reduction in HU-induced phosphorylation of RPA2 pS4/8 and pT21 in HeLa cells (Figures 6E, S6A), as previously reported (Liu et al., 2011). We also observed a reduction in RPA2 S33 phosphorylation (Figure 6E), which is thought to be mediated by ATR (Zeman and Cimprich, 2014). Importantly, we rescued impaired phosphorylation of all three sites by expression of siRNA-resistant RFWD3 (Figure 6E). Additionally, we observed defective RPA2 phosphorylation in mouse ES and U2OS cells using multiple siRNAs (Figures S6C, S6E, S6F).

Having shown that RFWD3 promotes RPA phosphorylation, we examined whether it regulates the phosphorylation of other ATR substrates. Two prior studies have investigated the dependence of CHK1 phosphorylation on RFWD3 and come to opposite conclusions. Using different cancer cell lines, one study found that RFWD3 depletion had no effect on HU-induced phosphorylation of CHK1 in HeLa cells (Liu et al., 2011) while the other observed a reduction in CHK1 phosphorylation in U2OS cells (Gong and Chen, 2011). We confirmed the findings of both studies in their respective cell lines, although the reduction in U2OS cells was not particularly strong (Figures S6A, S6B, S6D). Since this discrepancy may arise from peculiarities in cancer cell genotypes, we also examined CHK1 phosphorylation in primary diploid mouse embryonic stem cells used in our HR assays. We found that RFWD3 depletion partially inhibited HU-induced CHK1 S317 phosphorylation at 30 minutes yet did not impair CHK1 phosphorylation at 2 hours (Figure S6E, S6F). These findings suggest that RFWD3 may promote CHK1 phosphorylation in a cell type-specific fashion. They also suggest that RFWD3's roles in fork restart and HR, at least in HeLa and mouse ES cells, are unlikely to be mediated through activation of CHK1. As discussed below, RFWD3's role in promoting RPA phosphorylation may be related to its HR function.

Disruption of RPA ubiquitination inhibits homologous recombination at stalled replication forks

RFWD3 may promote HR through ubiquitination of RPA or another substrate. To distinguish between these possibilities, we sought to abolish RPA ubiquitination by a means other than RFWD3 depletion. We turned first to mutating RPA ubiquitination sites. All three

Author Manuscript Author Manuscript Author Manuscript Author Manuscript

subunits of the RPA complex are ubiquitinated in response to replication stress. It is possible that ubiquitination of all subunits is necessary for HR or that only one is the physiologic RFWD3 target and the others are ubiquitinated as bystanders. We noted that ubiquitination of RPA2 was consistently more robust than that of RPA1. We therefore sought to selectively abolish RPA2 ubiquitination. No sites of inducible RPA2 ubiquitination were detected in our proteomic screen, so we took a candidate approach in mutating sites. Regulatory phosphorylation of the RPA2 N-terminus suggested that it may provide the key surface through which post-translational modifications influence RPA activity. Only two lysines (K37 and K38) are located N-terminal to the OB-fold of RPA2 in proximity to its multiple phosphorylation sites (Figure S7A). Notably, we found that mutation of these lysines significantly decreased RPA2 ubiquitination in response to HU (Figure 7A). These sites may not have been detected by mass spectrometry as the tryptic peptide containing them may have been too long (Figure S7A).

Having identified K37 and K38 as putative RPA2 ubiquitination sites, we next evaluated their role in promoting the resolution of γH2AX foci and HR repair at stalled forks. HR. We depleted RPA2 with an siRNA targeting its 3′UTR and complemented cells with wild type or K37/38R RPA2. We found that K37/38R mutation did not significantly affect Tus-induced HR (Figure 7F) but delayed resolution of γH2AX foci after HU treatment (Figure 7E) and partially inhibited RPA phosphorylation (Figure S7B). These results provide evidence that RPA2 ubiquitination promotes repair at stalled forks but also suggest that RPA2 is not the sole target in this process and that ubiquitination of RPA1 and/or RPA3 play roles too. We therefore attempted to disrupt RPA1 ubiquitination by mutating all UV-induced RPA1 sites identified in our proteomic screens (Figure 1B). Surprisingly, simultaneous mutation of all 14 sites to arginine reduced but failed to abolish RPA1 ubiquitination (Figure 7B). These results indicate that among 41 lysines in RPA1, numerous alternative sites can substitute for those found in our screens. Consistent with the involvement of new acceptor lysines, the pattern of RPA1 ubiquitination was altered (Figure 7B).

Persistent RPA1 ubiquitination made it essentially impossible to generate a ubiquitination-resistant mutant through lysine mutation. We therefore took an alternative approach to eliminate RPA ubiquitination, one that would also inhibit RPA3 ubiquitination, which may additionally contribute to HR. We surmised that disrupting the interaction of RFWD3 with RPA would inhibit ubiquitination of the entire RPA complex. Interaction of RFWD3 with RPA is known to be abolished by deletion of 20 amino acids (residues 243–262) within the C-terminus of RPA2 (Gong and Chen, 2011). Notably, RPA2 lacking these residues is still capable of forming a trimeric complex with RPA1 and RPA3 and also binding ssDNA (Braun et al., 1997; Lee and Kim, 1995). We deleted these 20 residues from RPA2 and confirmed that their loss inhibited RFWD3 binding while having no effect on complex formation with RPA1 (Figure 7C) or on RPA2 localization to UV laser stripes (Figure S7C). Consistent with a role for RFWD3 in mediating RPA ubiquitination, deletion of these residues also inhibited HU-induced RPA ubiquitination (Figure 7D). Notably, their deletion additionally inhibited RPA2 phosphorylation, as observed by a decreased RPA2 mobility shift in lysates (Figure 7D).

Author Manuscript Author Manuscript Author Manuscript Author Manuscript

To examine the effect of the 243–262 deletion on DSB repair by HR, we depleted endogenous RPA2 and complemented cells with wild type or truncated RPA2 (Figures 7F, S7D, S7F). RPA2-depleted cells underwent significant cell death, resulting in increased basal γH2AX foci (Figure 7E) and basal phosphorylation of residual RPA2 on pS4/8 and pT21 (Figure S7F) in the absence of DNA damage. Reconstitution with wild type or truncated RPA2 rescued cell growth, diminished basal γH2AX foci (Figure 7E), and reduced basal phosphorylation of endogenous RPA2 (Figure S7F). Notably, deletion of residues 243–262 significantly delayed resolution of γH2AX foci after HU-induced damage (Figure 7E) and severely impaired homologous recombination at both Tus-stalled forks (Figure 7F) and I-SceI-induced DSBs (Figure S7E). It also abolished HU-induced phosphorylation of S33, T21, and S4/8 of RPA2 (Figure S7F). These results provide evidence independent of RFWD3 depletion that RPA ubiquitination promotes HR repair at stalled replication forks.

Discussion

RPA ubiquitination occurs in response to replication fork stalling

Using quantitative proteomics to profile DDR ubiquitination, we have demonstrated that all three subunits of the RPA complex are ubiquitinated on a minimum of 18 distinct sites in response to UV radiation. UV can cause replication fork stalling but can also induce replication-independent lesions repaired by NER. Importantly, RPA was also ubiquitinated in response to HU and aphidicolin, which cause fork stalling and polymerase-helicase uncoupling (Byun et al., 2005), suggesting that ssDNA is the trigger for RPA ubiquitination. Furthermore, HU-induced RPA ubiquitination was enhanced by ATR inhibition, suggesting that collapse of stalled forks may contribute to RPA ubiquitination. This finding points to a potential role for RPA ubiquitination in the repair of DSBs that arise at such forks. Notably, DSB-inducing agents that do not cause polymerase-helicase uncoupling, such as IR, did not activate RPA ubiquitination.

The fraction of RPA modified by ubiquitination is small, as indicated by our inability to detect RPA ubiquitination upon overexposure of lysate immunoblots. This suggests that ubiquitination occurs locally near DNA damage sites, and supporting this idea, RPA ubiquitination occurs exclusively on chromatin. Ubiquitination occurs on lysines that lie outside the DNA binding channel of RPA1, consistent with the model that RPA is bound to DNA when ubiquitination occurs. Because RPA ubiquitination occupancy is low, it would not be meaningful to examine the effects of proteasomal inhibition on bulk RPA levels. We therefore investigated MG132 effects on specifically the ubiquitinated RPA species. Induction of RPA ubiquitination by replication stress was inhibited by MG132, indicating that RPA ubiquitination does not lead to its proteasomal degradation and thus likely plays a role in signaling.

The E3 ligase RFWD3 mediates RPA ubiquitination

To determine the E3 ligase responsible for RPA ubiquitination, we identified candidate ligases interacting with RPA1 by mass spectrometry. While depleting these ligases and analyzing effects on RPA ubiquitination, we discovered a surprising artifact involving the inhibition of exogenous ubiquitin expression by siRNA transfection, which we suspect

Author Manuscript Author Manuscript Author Manuscript Author Manuscript

occurs through the interferon response. During the preparation of our manuscript, another study reported that the E3 ligase PRP19 ubiquitinates RPA (Marechal et al., 2014). We found that the siRNA utilized in their RPA ubiquitination experiments exhibited this artifact (Figure S4D). We evaluated four additional siRNAs and found one that depleted PRP19 but did not suppress the expression of exogenous ubiquitin substantially. Using this reagent, we were unable to detect an effect of PRP19 depletion on RPA ubiquitination. These results do not rule out a role for PRP19 in RPA ubiquitination, but given that the prior work did not examine exogenous ubiquitin expression nor perform a PRP19 rescue in their RPA ubiquitination experiments, we feel that PRP19's involvement in RPA ubiquitination remains to be firmly established. Notably, RFWD3 and PRP19 depletion result in similar defects in RPA phosphorylation, replication restart, and homologous recombination (Abbas et al., 2014; Marechal et al., 2014). It remains conceivable that both RFWD3 and PRP19 ubiquitinate RPA, with perhaps one ligase mediating monoubiquitination and the other polyubiquitin chain extension. Of note, while PRP19 is a splicing factor, we did not observe a reduction in RFWD3 protein levels upon PRP19 depletion and vice-versa (Figure S4F).

RFWD3 promotes replication fork restart and homologous recombination at stalled forks

Rapid disappearance of RPA ubiquitination upon release from HU-induced arrest suggested that RFWD3 may function in the stabilization or restart of stalled replication forks. Consistent with this idea, we found that RFWD3 promotes the restart of stalled forks using DNA fiber analysis. We also found that RFWD3 stimulates homologous recombination at stalled forks, which may contribute to its role in fork restart. HR factors have increasingly been implicated in the stabilization and restart of stalled forks (Hashimoto et al., 2010; Petermann et al., 2010; Schlacher et al., 2012). Supporting a role for RFWD3 in HR-mediated repair of DSBs at stalled forks, RFWD3 depletion delayed resolution of γ-H2AX foci after prolonged HU treatment. Ubiquitination of RPA may promote HR by facilitating its displacement from ssDNA to allow RAD51 filament formation. Alternatively, RPA ubiquitination may directly recruit RAD51 or other HR factors, as has been previously suggested to occur for both RPA sumoylation (Dou et al., 2010; Psakhye and Jentsch, 2012) and RPA phosphorylation (Lee et al., 2010; Shi et al., 2010; Wu et al., 2005). Dependence of RPA phosphorylation on RPA ubiquitination, which we demonstrated through both RFWD3 depletion and RPA mutation, may provide a mechanistic link through which RPA ubiquitination promotes HR. Lastly, RFWD3's function in HR may be unrelated to its roles in fork restart or stabilization, as observed for other HR factors (Petermann et al., 2010; Schlacher et al., 2011; Schlacher et al., 2012), and notably we found that RFWD3 also promotes HR away from stalled forks at I-SceI double-strand breaks (Figure 6C–D).

RFWD3 promotes multiple functions in the replication stress response that coincide with pathways regulated by ATR. Both homologous recombination and replication fork restart are known to be stimulated by ATR. Furthermore, we found that RFWD3 depletion caused an increase in new origin firing during replication stress (Figure S5E, S5G), suggesting that RFWD3 functions in the ATR-mediated intra S-phase checkpoint. Replication fork rates were also decreased in RFWD3-depleted cells in the absence of HU perturbation (Figure S5F), a phenotype known to occur upon inhibition of the ATR pathway (Petermann and Caldecott, 2006). While slower forks may delay ATR activation by HU-induced nucleotide

Author Manuscript Author Manuscript Author Manuscript Author Manuscript

pool depletion, we found that aphidicolin-induced RPA phosphorylation was also inhibited in RFWD3-depleted mouse ES cells (Figure S6G). Importantly, we found that RFWD3 depletion strongly inhibited RPA phosphorylation in all cell lines examined and partially impaired CHK1 phosphorylation in 2 of 3 lines. While RPA ubiquitination may promote ATR signaling, we can not rule out the possibility that it acts in cis to enhance the accessibility of RPA2 to phosphorylation or to prevent phosphatase binding. Why CHK1 phosphorylation variably depends on RFWD3 is unclear but may be due to a lower threshold for CHK1 phosphorylation by ATR in some contexts. The absence of a strong CHK1 phosphorylation defect in RFWD3-depleted HeLa and mouse ES cells prevents us from definitively concluding that RFWD3 promotes ATR activation. It also suggests that RFWD3 is unlikely to promote HR repair or fork restart through CHK1 in these cell lines, although it may involve other ATR substrates. Lastly, we found that RFWD3 depletion also increased basal CHK1 and CHK2 phosphorylation (Figures S6A, S6B, S6D) in the absence of DNA damage, consistent with a role for RFWD3 in promoting the stability of unperturbed replication forks. Thus RFWD3 may be necessary for both preventing and repairing DSBs arising during replication.

Multisite ubiquitination of the RPA complex promotes HR at stalled replication forks

Among the best-described pathways of ubiquitin-dependent signaling in the DDR are those involving the scaffold proteins H2AX, PCNA, and FANCD2/I. Ubiquitination of these proteins promotes DSB signal propagation, post replication repair, and interstrand crosslink repair, respectively. In each of these pathways, ubiquitination of specific lysine residues regulates DDR function. Our work now shows that HR repair at stalled replication forks is also linked to ubiquitination through the scaffold RPA. In this case, however, ubiquitination of numerous sites within multiple RPA subunits appears necessary for HR function. In this sense, RPA ubiquitination may represent an example of protein group modification, where individual sites do not serve unique functions but rather multisite ubiquitination of several proteins within a complex acts synergistically to promote a biological effect, as previously described for sumoylation of RPA and other HR factors in yeast (Psakhye and Jentsch, 2012)(Figure S7G). It is possible that decoration of the RPA complex with numerous ubiquitin moieties promotes weak interactions with cryptic ubiquitin binding domains in factors necessary for HR, as proposed for yeast RPA sumoylation (Psakhye and Jentsch, 2012). Alternatively, ubiquitination of RPA may regulate its recruitment to or release from DNA, as has been proposed for multisite XPC ubiquitination in NER (Poulsen et al., 2013; Sugasawa et al., 2005; van Cuijk et al., 2015). Whatever the mechanism, these results suggest that RFWD3-dependent RPA ubiquitination represents an important new step in the regulation of homologous recombination in the replication stress response.

Experimental Procedures

Purification of His-tagged ubiquitinated proteins

HeLa cells were transfected with pCS2 His-ubiquitin using HeLa MONSTER and TransIt reagents (MiRus). After 24 hr, they were treated with indicated DNA damage agents and harvested. Cell pellets were lysed in Buffer A (6 M Guanidine HCl, 100 mM NaH_2PO_4/Na_2HPO_4, 15 mM imidazole, pH 8 supplemented with 2 mM N-Ethylmaleimide) with

Author Manuscript Author Manuscript Author Manuscript Author Manuscript

sonication. Lysates were incubated with Ni-NTA agarose at room temperature for 3 hr. Bound complexes were washed once in Buffer A, twice in 1:3 Buffer (1 volume of Buffer A/3 volumes of TI Buffer), and finally once with TI Buffer (25 mM Tris, 20 mM imidazole, pH6.8). Beads were eluted in Laemmli sample buffer supplemented with 250 mM imidazole and boiled.

DNA fiber analysis

HeLa cells were transfected with RFWD3 or control siRNA. After 48 hr, they were then incubated with 25 μM IdU (Sigma, I7125) for 20 min and subsequently treated with 2 mM hydroxyurea for 2 hr. After washing out hydroxyurea, they were incubated with 250 μM CldU (Sigma, C6891) for 25 min. Cells were harvested and DNA fibers prepared on glass slides as previously described (Jackson and Pombo, 1998). Slides were incubated in 2.5 M HCl for 45 min and blocked in PBS with 1% BSA and 0.1% NP40. To detect CldU incorporation, fibers were stained with rat anti-BrdU (Abcam, ab6326) followed by Alexa Fluor® 488 Anti-Rat IgG (H+L) (Life Technologies, A-11006). To detect IdU incorporation, they were subsequently stained with mouse anti-BrdU (BD Biosciences, 347580) followed by Alexa Fluor® 594 Anti-Mouse IgG (H+L) (Life Technologies, A-21201). Pictures were taken with an Olympus FluoView™ FV1000 confocal microscope and were analyzed with ImageJ. More than 200 fibers were counted for each condition. In all figures, data represent the mean and standard deviation. P-values were calculated using a two-tailed unpaired t-test.

Homologous recombination assay

1.6×10^5 mouse 6xTer/HR ES cells were cotransfected in suspension with 0.30–0.35 μg pcDNA3β-myc NLS-I-SceI, pcDNA3β-myc NLS-Tus, or pcDNA3β-myc control vector along with either 20 pmol siLuc, RFWD3 siRNA, or RPA2 3′UTR siRNA using Lipofectamine 2000 (Invitrogen) as previously described (Willis et al., 2014). For RPA2 complementation experiments, transfections additionally included 0.1 μg plasmid containing wild type HA-RPA2, K37/38R HA-RPA2, truncated HA-RPA2 (‘Del’, lacking residues 243–262), or empty insert. In each experiment on a given day, GFP^+ frequencies were scored 72 hr after transfection by flow cytometry using a Becton Dickinson 5 Laser LSRII in duplicate and values corrected for background events and transfection efficiency. Approximately 6×10^5 total events were scored per sample. In all figures, data represent the mean and SEM of at least three experiments from different days (SEM = standard deviation/ $\sqrt{n}$, where n= number of experiments). P-values were calculated using a two-tailed unpaired t-test. Transfection efficiency ranged between 55%-95% and was measured by parallel transfection with 0.05 μg wild type *GFP* expression vector, 0.30 μg control vector, and 20 pmol siRNA.

Supplementary Material

Refer to Web version on PubMed Central for supplementary material.

Author Manuscript Author Manuscript Author Manuscript Author Manuscript

Acknowledgments

We thank members of the Elledge lab, L. Zou, and W. Harper for helpful discussions. We also thank L. Zou for the PRP19 stealth siRNA, J. Chen and Z. Gong for wild type and siRNA-resistant RFWD3 clones, Y. Wang for the RFWD3 antibody, and M. Rape for wild type, K63R, and K48R pCS2 His-ubiquitin plasmids. A.E.H.E is supported by a Burroughs Wellcome Fund CAMS Award and K12 Paul Calabresi Award for Oncology. I.H. is a recipient of an EMBO long-term fellowship. This work was supported by NIH grants to S.J.E., R.S. and S.P.G. S.J.E. is an Investigator with the Howard Hughes Medical Institute.

References

Abbas M, Shanmugam I, Bsaili M, Hromas R, Shaheen M. The role of the human psoralen 4 (hPso4) protein complex in replication stress and homologous recombination. J Biol Chem. 2014; 289:14009–14019. [PubMed: 24675077]

Adamson B, Smogorzewska A, Sigoillot FD, King RW, Elledge SJ. A genome-wide homologous recombination screen identifies the RNA-binding protein RBMX as a component of the DNA-damage response. Nat Cell Biol. 2012; 14:318–328. [PubMed: 22344029]

Bansbach CE, Betous R, Lovejoy CA, Glick GG, Cortez D. The annealing helicase SMARCAL1 maintains genome integrity at stalled replication forks. Genes Dev. 2009; 23:2405–2414. [PubMed: 19793861]

Bekker-Jensen S, Mailand N. The ubiquitin- and SUMO-dependent signaling response to DNA double-strand breaks. FEBS Lett. 2011; 585:2914–2919. [PubMed: 21664912]

Bochkarev A, Pfuetzner RA, Edwards AM, Frappier L. Structure of the single-stranded-DNA-binding domain of replication protein A bound to DNA. Nature. 1997; 385:176–181. [PubMed: 8990123]

Braun KA, Lao Y, He Z, Ingles CJ, Wold MS. Role of protein-protein interactions in the function of replication protein A (RPA): RPA modulates the activity of DNA polymerase alpha by multiple mechanisms. Biochemistry. 1997; 36:8443–8454. [PubMed: 9214288]

Byun TS, Pacek M, Yee MC, Walter JC, Cimprich KA. Functional uncoupling of MCM helicase and DNA polymerase activities activates the ATR-dependent checkpoint. Genes Dev. 2005; 19:1040–1052. [PubMed: 15833913]

Ciccia A, Bredemeyer AL, Sowa ME, Terret ME, Jallepalli PV, Harper JW, Elledge SJ. The SIOD disorder protein SMARCAL1 is an RPA-interacting protein involved in replication fork restart. Genes Dev. 2009; 23:2415–2425. [PubMed: 19793862]

Ciccia A, Elledge SJ. The DNA damage response: making it safe to play with knives. Mol Cell. 2010; 40:179–204. [PubMed: 20965415]

Dantuma NP, Groothuis TA, Salomons FA, Neefjes J. A dynamic ubiquitin equilibrium couples proteasomal activity to chromatin remodeling. J Cell Biol. 2006; 173:19–26. [PubMed: 16606690]

Doil C, Mailand N, Bekker-Jensen S, Menard P, Larsen DH, Pepperkok R, Ellenberg J, Panier S, Durocher D, Bartek J, et al. RNF168 binds and amplifies ubiquitin conjugates on damaged chromosomes to allow accumulation of repair proteins. Cell. 2009; 136:435–446. [PubMed: 19203579]

Dou H, Huang C, Singh M, Carpenter PB, Yeh ET. Regulation of DNA repair through deSUMOylation and SUMOylation of replication protein A complex. Mol Cell. 2010; 39:333–345. [PubMed: 20705237]

Elia AE, Boardman AP, Wang DC, Huttlin EL, Everley RA, Dephoure N, Zhou C, Koren I, Gygi SP, Elledge SJ. Quantitative Proteomic Atlas of Ubiquitination and Acetylation in the DNA Damage Response. Mol Cell. 2015

Fradet-Turcotte A, Canny MD, Escribano-Diaz C, Orthwein A, Leung CC, Huang H, Landry MC, Kitevski-LeBlanc J, Noordermeer SM, Sicheri F, et al. 53BP1 is a reader of the DNA-damage-induced H2A Lys 15 ubiquitin mark. Nature. 2013; 499:50–54. [PubMed: 23760478]

Gong Z, Chen J. E3 ligase RFWD3 participates in replication checkpoint control. J Biol Chem. 2011; 286:22308–22313. [PubMed: 21504906]

Harms JS, Splitter GA. Interferon-gamma inhibits transgene expression driven by SV40 or CMV promoters but augments expression driven by the mammalian MHC I promoter. Hum Gene Ther. 1995; 6:1291–1297. [PubMed: 8590733]

Author Manuscript Author Manuscript Author Manuscript Author Manuscript

Hashimoto Y, Ray Chaudhuri A, Lopes M, Costanzo V. Rad51 protects nascent DNA from Mre11-dependent degradation and promotes continuous DNA synthesis. Nat Struct Mol Biol. 2010; 17:1305–1311. [PubMed: 20935632]

Huen MS, Grant R, Manke I, Minn K, Yu X, Yaffe MB, Chen J. RNF8 transduces the DNA-damage signal via histone ubiquitylation and checkpoint protein assembly. Cell. 2007; 131:901–914. [PubMed: 18001825]

Jackson DA, Pombo A. Replicon clusters are stable units of chromosome structure: evidence that nuclear organization contributes to the efficient activation and propagation of S phase in human cells. J Cell Biol. 1998; 140:1285–1295. [PubMed: 9508763]

Jackson SP, Durocher D. Regulation of DNA damage responses by ubiquitin and SUMO. Mol Cell. 2013; 49:795–807. [PubMed: 23416108]

Lee DH, Pan Y, Kanner S, Sung P, Borowiec JA, Chowdhury D. A PP4 phosphatase complex dephosphorylates RPA2 to facilitate DNA repair via homologous recombination. Nat Struct Mol Biol. 2010; 17:365–372. [PubMed: 20154705]

Lee SH, Kim DK. The role of the 34-kDa subunit of human replication protein A in simian virus 40 DNA replication in vitro. J Biol Chem. 1995; 270:12801–12807. [PubMed: 7759535]

Liu S, Chu J, Yucer N, Leng M, Wang SY, Chen BP, Hittelman WN, Wang Y. RING finger and WD repeat domain 3 (RFWD3) associates with replication protein A (RPA) and facilitates RPA-mediated DNA damage response. J Biol Chem. 2011; 286:22314–22322. [PubMed: 21558276]

Mailand N, Bekker-Jensen S, Faustrup H, Melander F, Bartek J, Lukas C, Lukas J. RNF8 ubiquitylates histones at DNA double-strand breaks and promotes assembly of repair proteins. Cell. 2007; 131:887–900. [PubMed: 18001824]

Marechal A, Li JM, Ji XY, Wu CS, Yazinski SA, Nguyen HD, Liu S, Jimenez AE, Jin J, Zou L. PRP19 Transforms into a Sensor of RPA-ssDNA after DNA Damage and Drives ATR Activation via a Ubiquitin-Mediated Circuitry. Mol Cell. 2014; 53:235–246. [PubMed: 24332808]

Mattiroli F, Vissers JH, van Dijk WJ, Ikpa P, Citterio E, Vermeulen W, Marteijn JA, Sixma TK. RNF168 ubiquitinates K13-15 on H2A/H2AX to drive DNA damage signaling. Cell. 2012; 150:1182–1195. [PubMed: 22980979]

Messick TE, Greenberg RA. The ubiquitin landscape at DNA double-strand breaks. J Cell Biol. 2009; 187:319–326. [PubMed: 19948475]

Nejepinska J, Flemr M, Svoboda P. Control of the interferon response in RNAi experiments. Methods Mol Biol. 2012; 820:133–161. [PubMed: 22131030]

Petermann E, Caldecott KW. Evidence that the ATR/Chk1 pathway maintains normal replication fork progression during unperturbed S phase. Cell Cycle. 2006; 5:2203–2209. [PubMed: 16969104]

Petermann E, Helleday T. Pathways of mammalian replication fork restart. Nat Rev Mol Cell Biol. 2010; 11:683–687. [PubMed: 20842177]

Petermann E, Orta ML, Issaeva N, Schultz N, Helleday T. Hydroxyurea-stalled replication forks become progressively inactivated and require two different RAD51-mediated pathways for restart and repair. Mol Cell. 2010; 37:492–502. [PubMed: 20188668]

Poulsen SL, Hansen RK, Wagner SA, van Cuijk L, van Belle GJ, Streicher W, Wikstrom M, Choudhary C, Houtsmuller AB, Marteijn JA, et al. RNF111/Arkadia is a SUMO-targeted ubiquitin ligase that facilitates the DNA damage response. J Cell Biol. 2013; 201:797–807. [PubMed: 23751493]

Psakhye I, Jentsch S. Protein group modification and synergy in the SUMO pathway as exemplified in DNA repair. Cell. 2012; 151:807–820. [PubMed: 23122649]

Schlacher K, Christ N, Siaud N, Egashira A, Wu H, Jasin M. Double-strand break repair-independent role for BRCA2 in blocking stalled replication fork degradation by MRE11. Cell. 2011; 145:529–542. [PubMed: 21565612]

Schlacher K, Wu H, Jasin M. A distinct replication fork protection pathway connects Fanconi anemia tumor suppressors to RAD51-BRCA1/2. Cancer Cell. 2012; 22:106–116. [PubMed: 22789542]

Shi W, Feng Z, Zhang J, Gonzalez-Suarez I, Vanderwaal RP, Wu X, Powell SN, Roti Roti JL, Gonzalo S, Zhang J. The role of RPA2 phosphorylation in homologous recombination in response to replication arrest. Carcinogenesis. 2010; 31:994–1002. [PubMed: 20130019]

Author Manuscript Author Manuscript Author Manuscript Author Manuscript

Sirbu BM, Cortez D. DNA damage response: three levels of DNA repair regulation. Cold Spring Harb Perspect Biol. 2013; 5:a012724. [PubMed: 23813586]

Sorensen CS, Hansen LT, Dziegielewski J, Syljuasen RG, Lundin C, Bartek J, Helleday T. The cell-cycle checkpoint kinase Chk1 is required for mammalian homologous recombination repair. Nat Cell Biol. 2005; 7:195–201. [PubMed: 15665856]

Stewart GS, Panier S, Townsend K, Al-Hakim AK, Kolas NK, Miller ES, Nakada S, Ylanko J, Olivarius S, Mendez M, et al. The RIDDLE syndrome protein mediates a ubiquitin-dependent signaling cascade at sites of DNA damage. Cell. 2009; 136:420–434. [PubMed: 19203578]

Sugasawa K, Okuda Y, Saijo M, Nishi R, Matsuda N, Chu G, Mori T, Iwai S, Tanaka K, Tanaka K, et al. UV-induced ubiquitylation of XPC protein mediated by UV-DDB-ubiquitin ligase complex. Cell. 2005; 121:387–400. [PubMed: 15882621]

Toledo LI, Altmeyer M, Rask MB, Lukas C, Larsen DH, Povlsen LK, Bekker-Jensen S, Mailand N, Bartek J, Lukas J. ATR prohibits replication catastrophe by preventing global exhaustion of RPA. Cell. 2013; 155:1088–1103. [PubMed: 24267891]

van Cuijk L, van Belle GJ, Turkyilmaz Y, Poulsen SL, Janssens RC, Theil AF, Sabatella M, Lans H, Mailand N, Houtsmuller AB, et al. SUMO and ubiquitin-dependent XPC exchange drives nucleotide excision repair. Nat Commun. 2015; 6:7499. [PubMed: 26151477]

Wang H, Wang H, Powell SN, Iliakis G, Wang Y. ATR affecting cell radiosensitivity is dependent on homologous recombination repair but independent of nonhomologous end joining. Cancer Res. 2004; 64:7139–7143. [PubMed: 15466211]

Willis NA, Chandramouly G, Huang B, Kwok A, Follonier C, Deng C, Scully R. BRCA1 controls homologous recombination at Tus/Ter-stalled mammalian replication forks. Nature. 2014; 510:556–559. [PubMed: 24776801]

Wu X, Yang Z, Liu Y, Zou Y. Preferential localization of hyperphosphorylated replication protein A to double-strand break repair and checkpoint complexes upon DNA damage. Biochem J. 2005; 391:473–480. [PubMed: 15929725]

Xu X, Vaithiyalingam S, Glick GG, Mordes DA, Chazin WJ, Cortez D. The basic cleft of RPA70N binds multiple checkpoint proteins, including RAD9, to regulate ATR signaling. Mol Cell Biol. 2008; 28:7345–7353. [PubMed: 18936170]

Yuan J, Ghosal G, Chen J. The annealing helicase HARP protects stalled replication forks. Genes Dev. 2009; 23:2394–2399. [PubMed: 19793864]

Yusufzai T, Kong X, Yokomori K, Kadonaga JT. The annealing helicase HARP is recruited to DNA repair sites via an interaction with RPA. Genes Dev. 2009; 23:2400–2404. [PubMed: 19793863]

Zeman MK, Cimprich KA. Causes and consequences of replication stress. Nat Cell Biol. 2014; 16:2–9. [PubMed: 24366029]

Zou L, Elledge SJ. Sensing DNA damage through ATRIP recognition of RPA-ssDNA complexes. Science. 2003; 300:1542–1548. [PubMed: 12791985]

Zou L, Liu D, Elledge SJ. Replication protein A-mediated recruitment and activation of Rad17 complexes. Proc Natl Acad Sci U S A. 2003; 100:13827–13832. [PubMed: 14605214]

Author Manuscript Author Manuscript Author Manuscript Author Manuscript

Highlights

- RPA is ubiquitinated on chromatin in response to replication fork stalling
- Ubiquitination of RPA is mediated by the E3 ligase RFWD3
- RFWD3 promotes replication fork restart and homologous recombination at stalled forks
- Multisite ubiquitination of the entire RPA complex is necessary for HR

Author Manuscript Author Manuscript Author Manuscript Author Manuscript

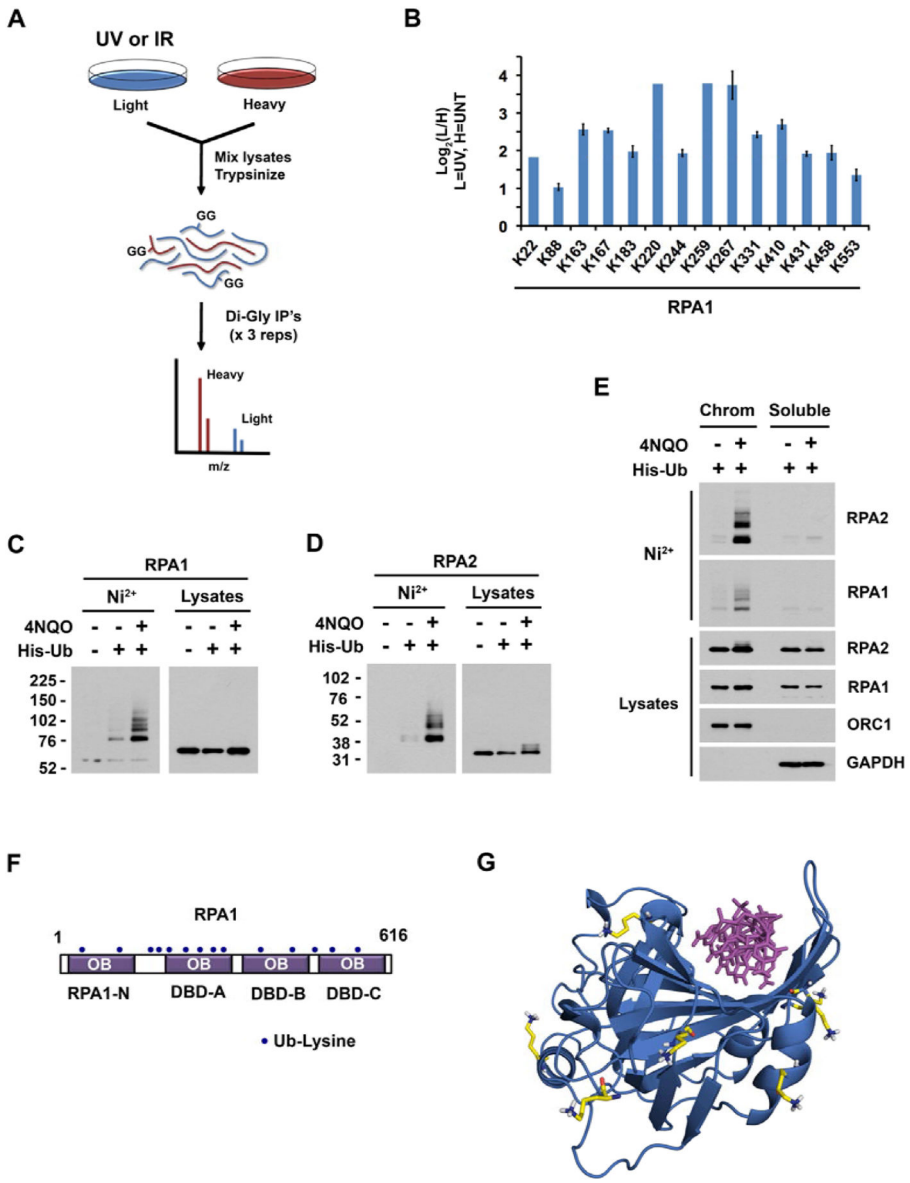

Figure 1. RPA is ubiquitinated on chromatin in response to UV radiation

(A) Schematic representation of proteomic approach to profile UV- or IR-regulated ubiquitination. Figure was adapted from our companion paper (Elia et al., 2015).

(B) Log_2(L/H) ratios for diGly sites on RPA1 induced by UV in the ubiquitin profiling experiments in Figures 1A or S1A. Error bars represent the SEM of unique MS1 quantifications.

(C, D) HeLa cells transfected with His-ubiquitin were treated with 1 μg/mL 4NQO for 2 hr. Nuclei were then purified and lysed under denaturing conditions. Nickel-purified proteins were immunoblotted for endogenous RPA1 or RPA2.

(E) HeLa cells transfected with His-ubiquitin were treated with 1 μg/mL 4NQO for 2 hr and then fractionated into chromatin and soluble extracts. Nickel purified proteins were blotted for endogenous RPA1 and RPA2.

Author Manuscript Author Manuscript Author Manuscript Author Manuscript

(F) RPA1 domain architecture, consisting of 4 OB-folds, three of which (DBD-A, DBD-B, and DBD-C) bind DNA. Dark blue circles represent sites of UV-induced ubiquitination in Figure 1B.

(G) Co-crystal structure of ssDNA bound to DBD-A and DBD-B of RPA1 (PDB entry 1JMC). UV-induced sites of ubiquitination (lysines shown in yellow) lie outside the DNA-binding channel. See also Figures S1, S2.

Author Manuscript Author Manuscript Author Manuscript Author Manuscript

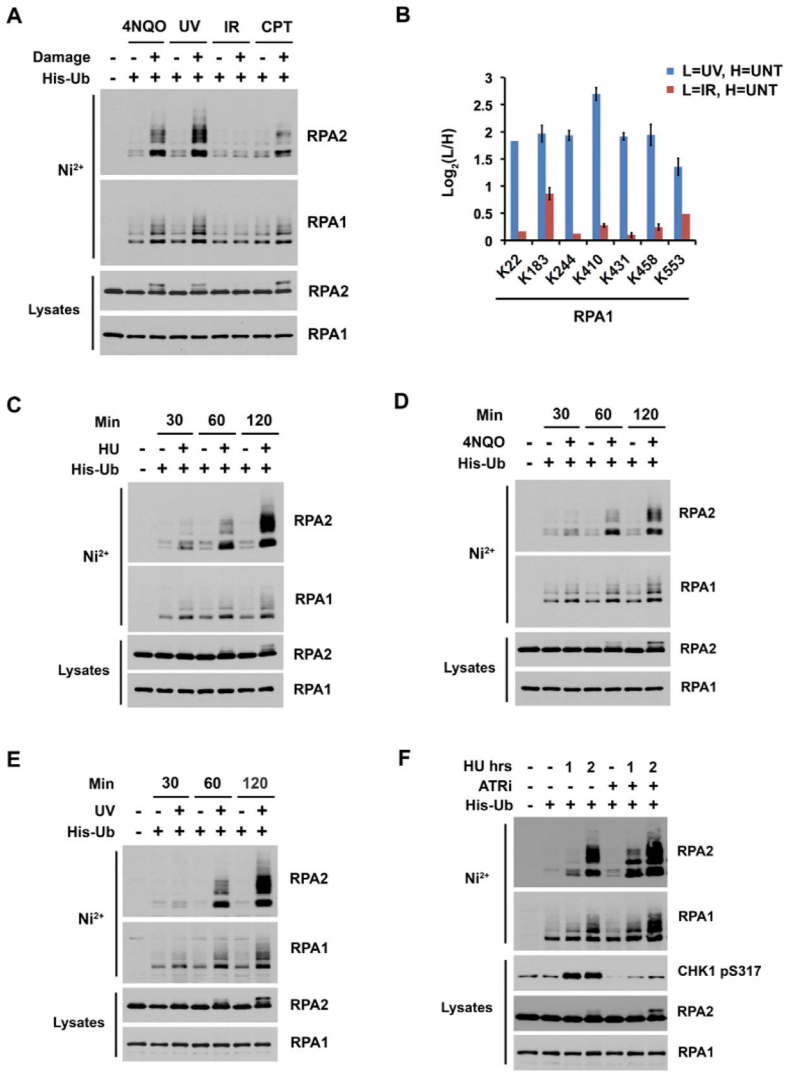

Figure 2. Kinetics of RPA ubiquitination in response to agents that cause polymerase-helicase uncoupling

(A) HeLa cells were treated with 1 μg/mL 4NQO, 30 J/m2 UV, 10 Gy IR, or 1 μM CPT and harvested 1 hr later. His-tagged ubiquitinated proteins purified from whole cell lysates were blotted for endogenous RPA1 or RPA2.

(B) Log_2(L/H) ratios for diGly sites on RPA1 that were quantified in both the UV and IR profiling experiments in Figures 1A or S1A. Error bars represent the SEM of unique MS1 quantifications.

(C) HeLa cells were treated with 2 mM HU and harvested after the indicated times. His-tagged ubiquitinated proteins purified from whole cell lysates were blotted for endogenous RPA1 and RPA2.

(D–E) Same as Figure 2C but cells were treated with 1 μg/mL 4NQO (Figure 2D) or 30 J/m^2 UV (Figure 2E) for the indicated times.

(F) HeLa cells were pre-treated with 10 μM ATR inhibitor (Vertex compound 45) for 30 min. HU at 2 mM was then added to the media, and the cells were harvested at 1 or 2 hr

Author Manuscript Author Manuscript Author Manuscript Author Manuscript

later. His-tagged ubiquitinated proteins purified from whole cell lysates were blotted for endogenous RPA1 and RPA2. See also Figure S1.

Author Manuscript Author Manuscript Author Manuscript Author Manuscript

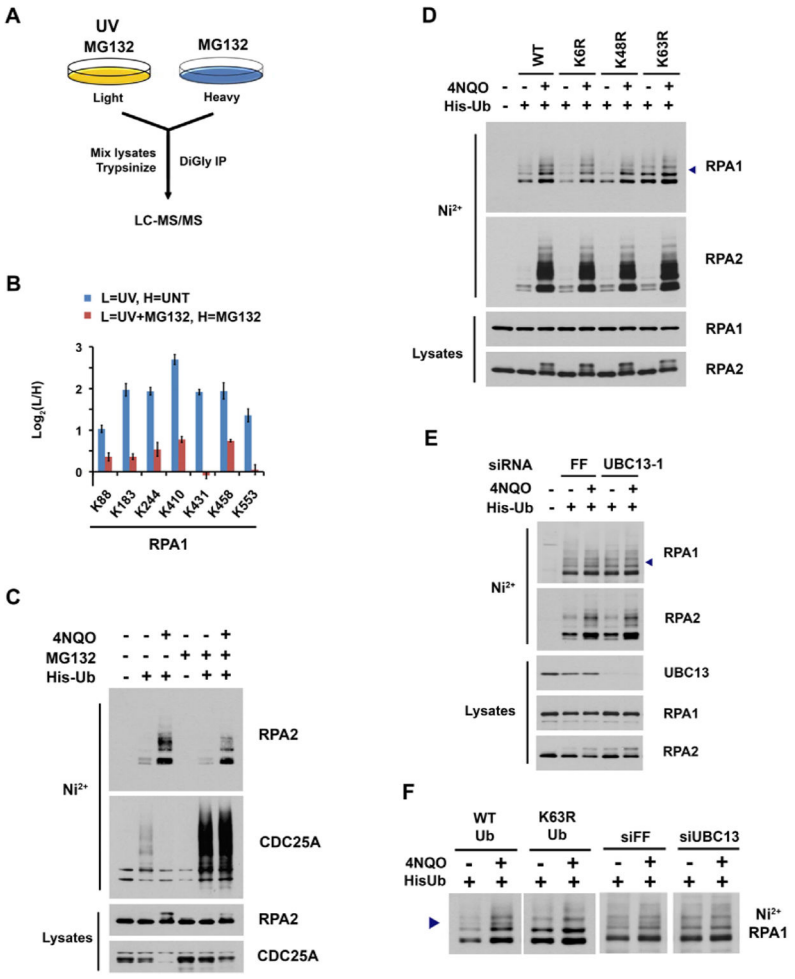

Figure 3. RPA ubiquitination does not lead to its degradation by the proteasome

(A) Schematic overview of UV and IR ubiquitin profiling in the presence of proteasome inhibition. Figure was adapted from our companion paper (Elia et al., 2015).

(B) Log_2(L/H) ratios for diGly sites on RPA1 that were quantified in both the UV (Figure 1A) and UV-MG132 (Figure 3A) proteomic experiments. Error bars represent the SEM of unique MS1 quantifications.

(C) HeLa cells were pre-treated with 5 μM MG132 for 2 hr. 4NQO was then added to the media at 1 μg/mL, and cells were harvested 2 hr later. His-tagged ubiquitinated proteins were purified and blotted for endogenous RPA2 and CDC25A.

(D) HeLa cells transfected with wild type His-ubiquitin or various His-ubiquitin mutants (K6R, K48R, K63R) were treated with 1 μg/mL 4NQO and harvested 2 hr later. Nickel-purified proteins were blotted for endogenous RPA1 and RPA2. Arrowhead represents a ubiquitinated RPA1 band that disappears upon ubiquitin K63R mutation or UBC13 depletion (Figures 3F, 3E, S3F–G). His-ubiquitin loading control is provided in Figure S3E.

(E) HeLa cells were transfected with siUBC13-1 or control siFF. One day later, they were transfected with His-ubiquitin and then treated 24 hr later with 1 μg/mL 4NQO for 2 hr. Nickel purified proteins were blotted for endogenous RPA1 and RPA2. Arrowhead same as Figure 3D.

Author Manuscript Author Manuscript Author Manuscript Author Manuscript

(F) Magnified view of ubiquitinated RPA1 (detected in Figures 3D and 3E) to demonstrate loss of ubiquitinated band (indicated by arrowhead) upon ubiquitin K63R mutation or UBC13 depletion. See also Figure S3.

Author Manuscript Author Manuscript Author Manuscript Author Manuscript

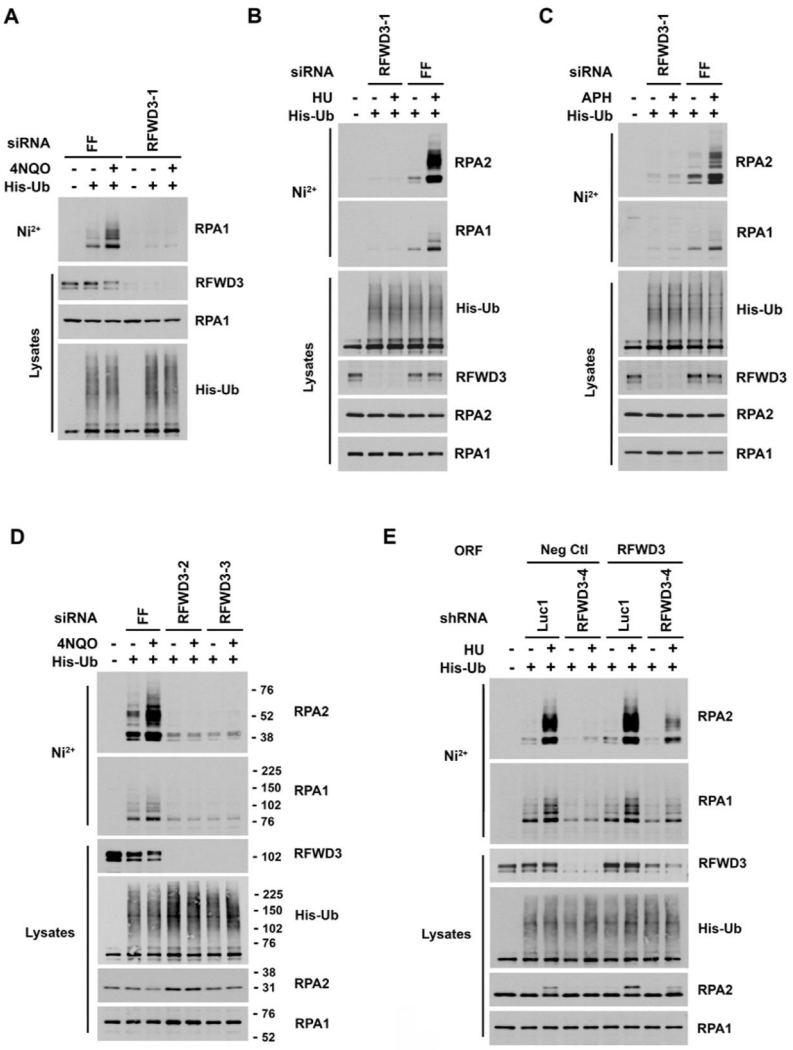

Figure 4. The ubiquitin ligase RFWD3 mediates RPA ubiquitination

(A–D) HeLa cells were transfected with control siFF or the indicated siRNAs against RFWD3. One day later, they were transfected with His-ubiquitin and then treated 24 hr later with 1 μg/mL 4NQO, 2 mM HU, or 30 μM aphidicolin for 2 hr. Nickel purified proteins were blotted for endogenous RPA1 and/or RPA2.

(E) HeLa cells were transduced with shRFWD3-4 or non-targeting shLuc1 along with either shRNA-resistant RFWD3 or negative control empty vector. They were then transfected with His-ubiquitin and treated 24 hr later with 2 mM HU for 2 hr. Nickel-purified proteins were blotted for endogenous RPA1 and RPA2. See also Figure S4.

Author Manuscript Author Manuscript Author Manuscript Author Manuscript

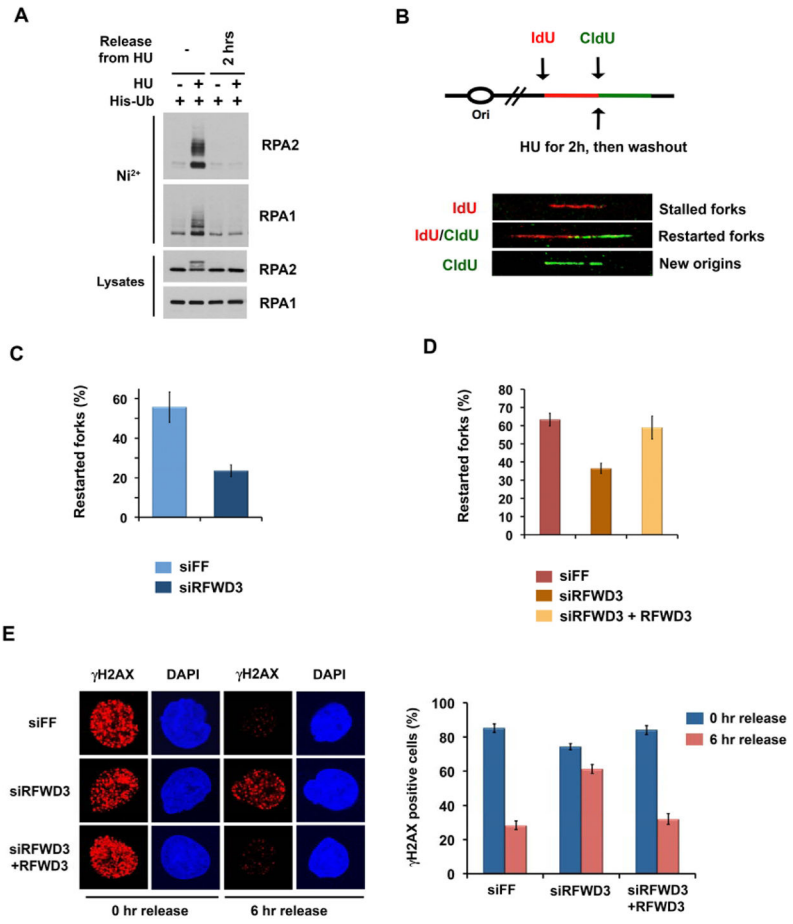

Figure 5. RFWD3 promotes replication fork restart and DNA repair at stalled replication forks

(A) HeLa cells transfected with His-ubiquitin were treated with 2 mM HU for 2 hr followed by no release or a release of 2 hr. Nickel purified proteins were blotted for endogenous RPA1 and RPA2.

(B) Schematic of the pulse-labeling experiment for DNA fiber analysis. DNA fibers were stained with antibodies recognizing IdU (red) and CldU (green). Restarted forks are indicated by red tracts followed by green tracts.

(C) Percentage of restarted forks in HeLa cells transfected with siRFWD3-4 or control siFF and treated according to Figure 5B. Data represent the mean and standard deviation (n=4, p=0.0017, t-test).

(D) HeLa cells expressing siRNA-resistant RFWD3 were transfected with siRFWD3-4 and compared to HeLa cells transfected with siFF or siRFWD3-4. Cells were treated according to Figure 5B and percentage of restarted forks measured. Data represent the mean and standard deviation (n=3, p=0.0005 for siFF vs. siRFWD3, p=0.0049 for siRFWD3 vs. siRFWD3+RFWD3, t-test).

(E) HeLa cells expressing siRNA-resistant RFWD3 were transfected with siRFWD3-4 and compared to HeLa cells transfected with siFF or siRFWD3-4. Cells were treated with 200 μM HU for 24 hr, released for the indicated times, and immunostained for γH2AX foci. Data represent the mean and standard deviation for the percentage of cells with more than 10

Author Manuscript Author Manuscript Author Manuscript Author Manuscript

γH2AX foci. (n=3, p=0.0002 for siFF vs. siRFWD3 at 6 hr, p=0.0003 for siRFWD3 vs. siRFWD3+RFWD3 at 6 hr, t-test). See also Figure S5.

Author Manuscript Author Manuscript Author Manuscript Author Manuscript

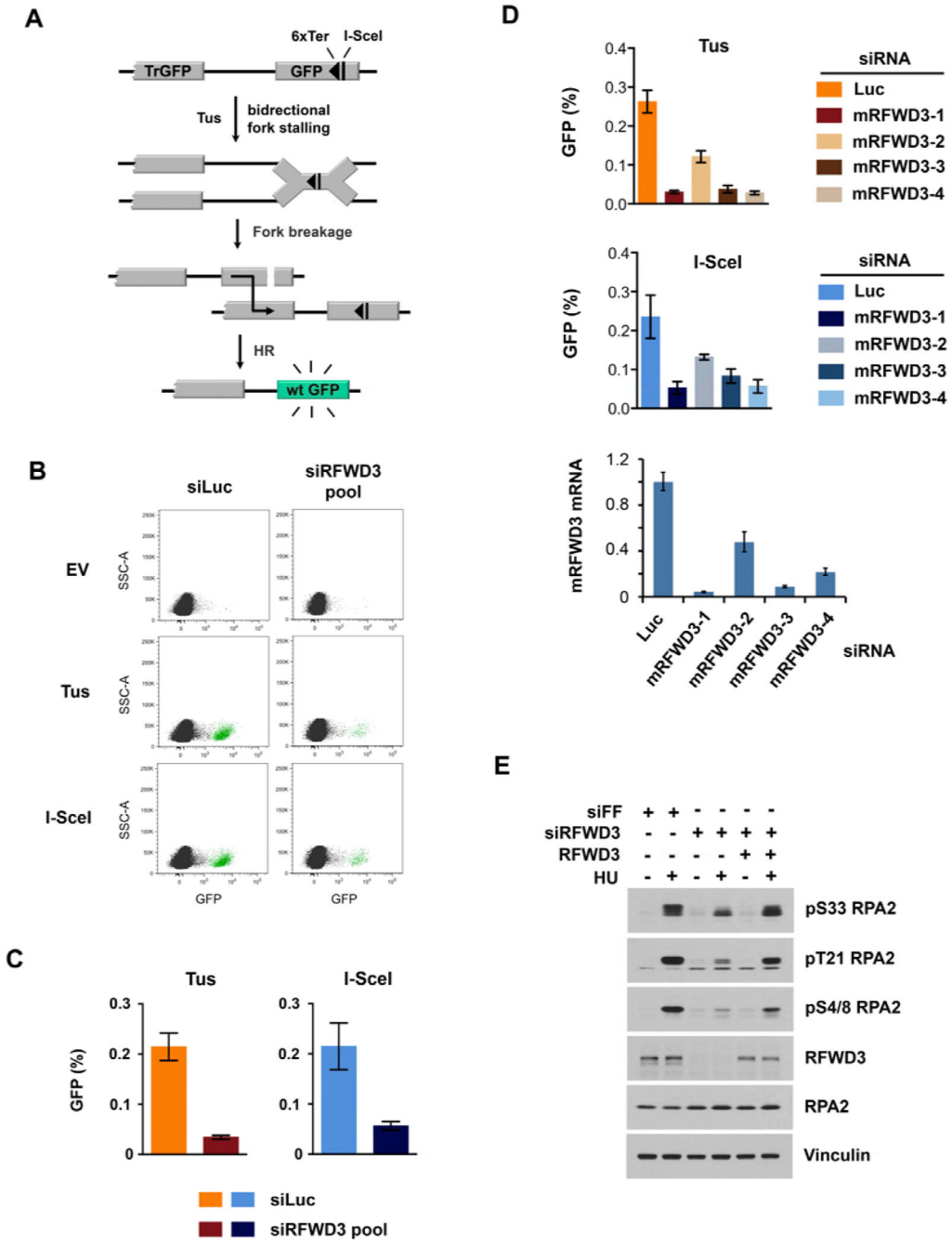

Figure 6. RFWD3 promotes homologous recombination at stalled replication forks

(A) Schematic of the Tus/6xTer homologous recombination reporter. TrGFP indicates truncated GFP. Triangle represents the 6xTer site adjacent to an I-SceI site.

(B) Flow cytometry plots in mouse 6xTer/HR cells co-transfected with empty-vector, Tus, or I-SceI and with either control siLuc or mouse siRFWD3 pool. Plots represent raw FACS data for a single representative experiment. Quantitation for all experiments (n=7) is given in Figure 6C.

Author Manuscript Author Manuscript Author Manuscript Author Manuscript

(C, D) Homologous recombination frequencies in mouse 6xTer/HR cells co-transfected with Tus or I-SceI and either control siLuc, mouse siRFWD3 pool, or 1 of 4 individual mouse RFWD3 siRNAs. Data represent the mean and SEM. (Figure 6C, n=7, p=0.0005 for Tus, p=0.014 for I-SceI, t-test) (Figure 6D, n=3, $p<0.05$ for all Tus pairwise siLuc vs. each siRFWD3, p= 0.05–0.10 for all I-SceI pairwise siLuc vs. each siRFWD3, t-test). Below is RT-qPCR analysis of RFWD3 mRNA in mouse 6xTer/HR cells transfected with siLuc or indicated siRNAs against mouse RFWD3.

(E) HeLa cells expressing siRNA-resistant RFWD3 were transfected with siRFWD3-4 and compared to HeLa cells transfected with siFF or siRFWD3-4. Cells were treated with 2 mM HU for 2 hr, and lysates were blotted with RPA2 phosphospecific antibodies. See also Figures S5, S6.

Author Manuscript Author Manuscript Author Manuscript Author Manuscript

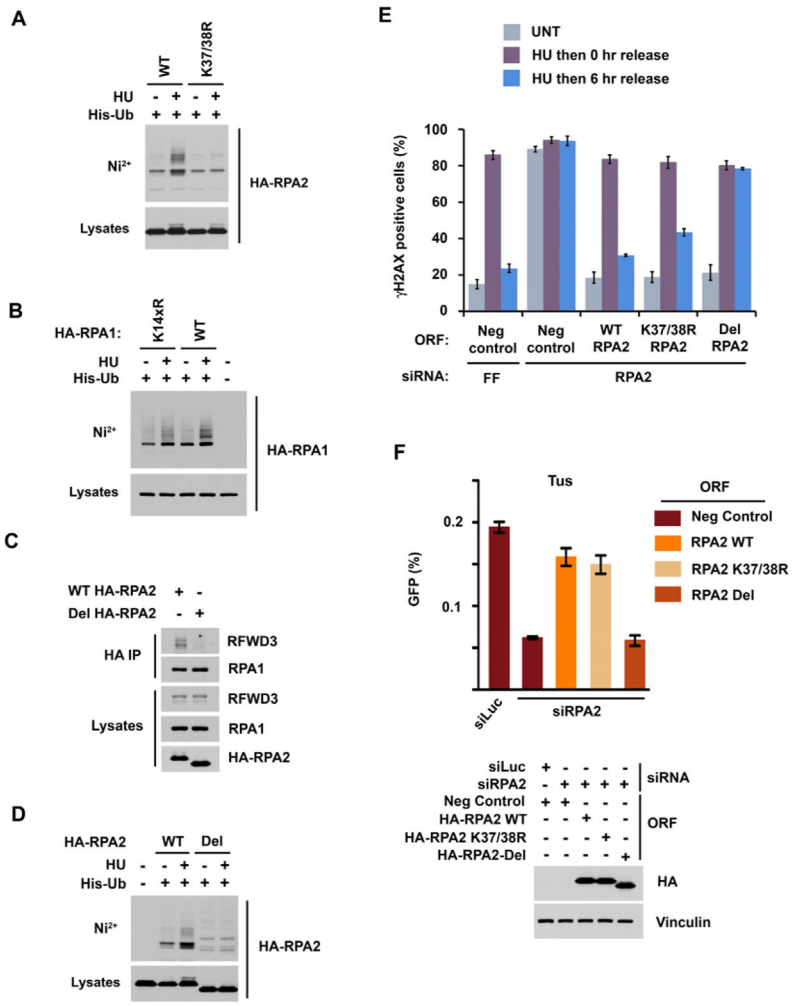

Figure 7. Disruption of RPA ubiquitination inhibits homologous recombination repair at stalled replication forks

(A) HeLa cells expressing wild type or K37/38R HA-RPA2 and His-ubiquitin were treated with 2 mM HU for 2 hr and nickel-purified proteins immunoblotted with HA antibody.

(B) HeLa cells expressing wild type or K14xR HA-RPA1 and His-ubiquitin were treated with 2 mM HU for 2 hr and nickel-purified proteins immunoblotted with HA antibody. K14xR represents mutation of the 14 regulated sites in Figure 1B.

(C) HeLa cells expressing wild type or truncated (lacking residues 243–262, “Del”) HA-RPA2 were treated with 2 mM HU for 2 hr and HA immunoprecipitates blotted for endogenous RFWD3 and RPA1.

(D) HeLa cells expressing wild type or “Del” HA-RPA2 and His-ubiquitin were treated with 2 mM HU for 2 hr and nickel-purified proteins immunoblotted with HA antibody.

(E) HeLa cells expressing non-tagged wild type RPA2, K37/38R RPA2, “Del” RPA2, or negative control empty vector were transfected with siFF or an siRNA targeting the 3′ UTR of RPA2. Cells were treated with 200 μM HU for 24 hr, released for the indicated times, and immunostained for γH2AX foci (n=3, p=0.024 for WT vs. K37/38R at 6 hr, p=0.003 for WT vs. Del at 6 hr, p=0.016 for K37/38R vs. Del at 6 hr, t-test).

Author Manuscript Author Manuscript Author Manuscript Author Manuscript

(F) Homologous recombination frequencies in mouse 6xTer/HR cells co-transfected with Tus and with either siLuc or an siRNA targeting the 3′ UTR of RPA2. Cells were also co-transfected with either wild type HA-RPA2, K37/38R HA-RPA2, “Del” HA-RPA2, or negative control empty vector. HA immunoblot shows equivalent expression of RPA2 constructs (n=4, p=0.0002 for WT vs. Del, p=0.0003 for K37/38R vs. Del, p=0.46 for WT vs. K37/38R). See also Figure S7.